Macromolecules

pubs.acs.org/Macromolecules Article

Bound Layer Polymer Behavior on Graphene and Graphene Oxide Nanosheets

Georgios Kritikos,* Anastassia N. Rissanou,* Vagelis Harmandaris, and Kostas Karatasos

Cite This: *Macromolecules* 2020, 53, 6190–6203 Read Online

ACCESS | Metrics & More | Article Recommendations | Supporting Information

ABSTRACT: Molecular dynamics simulations were employed to study the bound layer in polymer/graphene-based nanocomposites. We focused on the dynamic behavior of polar (poly(acrylic acid)) and nonpolar (polystyrene) linear chains, at the interface with graphene-based fillers, bearing different affinities with the polymers and different nanoroughness. Four temperatures were examined with a step of 50 K and the lowest one 100 K above the T_g of the corresponding bulk polymers. The dynamic response of the adsorbed layer exhibited an increased departure from that of the bulk, accompanied by a higher degree of dynamical heterogeneity, especially for the oxidized graphene systems. In the case of the nonoxidized analogues, an increased anisotropy of polymer diffusion parallel and perpendicular to the filler's plane was observed. Dynamics within the adsorbed layer exhibited Arrhenius-like characteristics in all the examined systems, in agreement with recent experimental studies. The combination of the results associated with backbone torsional motion and the chain desorption process revealed a strong dynamic transition near both the examined nanosheets, almost 100 K above the bulk T_g. However, in the adjacent-to-the-adsorbed layer, polymer dynamic characteristics approached the bulk behavior. It is therefore implied that, depending on its average size, a polymer chain may experience different dynamic regimes across its length near the interface region.

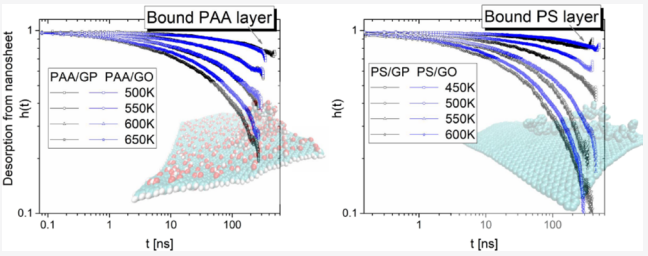

I. INTRODUCTION

Polymer/graphene composite materials are used nowadays in a wide range of applications.[1−6] Because of the extended polymer/filler interface, inclusion of a small percentage (∼1 wt %) of pristine graphene (GP) or graphene oxide (GO) nanosheets can trigger dramatic changes in the polymer matrix behavior.[1−4] Enhanced/modified properties (i.e., thermal, electronic, mechanical, etc.) are the result of the interaction between polymer chains and graphene sheets as well as the chemical structure of the monomers, the molecular weight (chain length), the structure at the polymer/graphene interface, the crystallinity, and interchain interactions.[7,8] Various polymer properties in the proximity of polymer/solid interfaces differ from their bulk values.[9−13] The way that the polymer/graphene interface affects the properties of the polymer chains, as well as the estimation of the width of the interphase, based on the specific property under study is of particular importance.[14,15]

Usually, mixing of the one-atom-thick graphene flakes[2] with bulk polymer leads to an increase of the glass transition temperature (T_g),[3,16] although cases of a reduction in the T_g have also been reported.[17] Semicrystallization is also affected since GP-based sheets can promote heterogeneous crystallization, resulting in an increase in the crystallization temperature (T_c).[8,15,17,18] Based on such effects, tuning of mechanical, thermal, electrical, and permeability properties can be performed[2,16,19−22] to meet specific needs in materials technology.

Among the most frequently used polymers in GP-based nanocomposites is polystyrene (PS). PS is a nonpolar macromolecular matrix which upon mixing with GP-based fillers may acquire desirable attributes, such as an electrical response appropriate for applications in energy,[23] anticorrosion properties,[24] electronic properties that can be exploited in the fabrication of electronic parts,[25,26] properties appropriate for use as a magnetic material,[27] and so on. For instance, the percolation threshold for electrical conductivity in PSGO systems was estimated to be close to 0.1 vol % in GO,[2,4] while mechanical reinforcement resulting in a 70% increase in the tensile strength[28] appears even at low filler contents (∼1 wt %) in GP.

Another polymer that has recently been studied as a polar matrix in GO-based nanocomposites is poly(acrylic acid) (PAA).[29,30] PAA is a polyelectrolyte which in an aqueous environment becomes ionized and can form membranes with

Received: May 1, 2020
Revised: June 12, 2020
Published: July 24, 2020

https://dx.doi.org/10.1021/acs.macromol.0c01040
Macromolecules 2020, 53, 6190−6203

nanosized channels for energy or water purification applications.[31−33] The presence of GO acts toward improving the mechanical stability and the electrical properties of PAA hydrogels.[30,34,35] Even at very low GO contents (i.e., close to 0.05 wt %), a percolated interphase[3] can be developed, which results in an enhanced mechanical and thermal behavior compared to that of conventional hydrogels.

Irrespective of the polar or nonpolar nature of the polymeric matrix, the formation of a bound polymer layer takes place,[15,16,36−40] within which polymer chains appear to undergo a dynamic transition to a rigid amorphous phase.[15] This transition is detected by the reduction of the dielectric strength in dielectric relaxation spectroscopy (DRS) experiments[17,36,41] and the reduction of the heat capacity step in differential scanning calorimetry (DSC) experiments.[15,17,41] It is widely accepted that the dynamics of the bulk polymer fraction, when entering the α-relaxation regime, follows the Vogel−Fulcher−Tammann (VFT)[42−44] behavior, which is characterized by an increase in the activation energy. The explanation is based on the cooperative characteristics of the diffusion.[45−47] However, the bound layer dynamics, in the same regime, follows an Arrhenius-like behavior of almost constant activation energy.[17,41,48−50] An interpretation of this phenomenon attributes it to the suppression of the cooperative characteristics of the diffusion at the polymer/solid interface, when the confinement length is shorter than the cooperative length.[46,49,51−54] Another interpretation is based on an extension of the glassy region of cooperative dynamics and a "stronger" transition on the nanofiller compared to the bulk.[15,55] In this case the adhesion tension follows a quadratic temperature dependence, implying a linear reduction of the entropy of the bound layer and thus the absence of a heat capacity step.[15] A complex dynamical behavior of chains at the interface has been reported as a result of an interplay between the conformational entropy of polymer chains and the adhesive interaction between the polymer and the substrate.[56−61]

Atomistic molecular dynamics (MD) simulations have been extensively utilized for the study of polymer/solid interfaces[8,39,70,62−69] as they can offer a finer temporal and spatial resolution compared to commonly used experimental techniques. The filler's surface functionalization and the atomic-scale roughness can be represented in detail,[13,62,63] and the pertinent adsorption/desorption phenomena can be monitored within time scales reaching the microseconds range.[29,65,66,71] Such computational studies have shown that chain stereochemistry and stiffness are important parameters that affect the prevailing configurations on the polymer/solid interface.[61,71−73] Stiffer chains usually form shorter loops, while the larger part of the adsorbed chain is distributed in tails.[15,74] In addition, global chain dimensions are expected to be affected by the ratio of the size of the nanofiller to that of the polymer and the induced confinement conditions.[75,76]

In this study, the formation of a dynamically arrested interfacial polymer layer close to the graphene surface was explored through a detailed analysis of the structural characteristics and the dynamical properties of the systems. Particular emphasis was placed in the role of the roughness of the filler and the presence of specific interactions between the filler and the polymer matrix (e.g., hydrogen-bonding and $\pi-\pi$ interactions), associated with the physically adsorbed polymer layer. For this reason, detailed atomistic MD simulations were performed in different graphene-based polymer nanocomposites. In these systems, nanosheets with inherently different degree of roughness in the nanoscale and polymer matrices with different affinities with the fillers have been considered. To simulate conditions that represent a good dispersion of the filler within the polymer matrix, a single nanosheet was immersed in a simulation box filled by several hundreds of polymer chains. This resulted in composites between 0.5 and 1.0 wt % in the nanofiller. The temperature (T) dependence has also been examined through a series of simulation runs at different temperatures. For both polymer matrices the examined T range is well above the corresponding T_g of the bulk polymers, with the lowest temperature being ∼100 K higher.

In section II, details of the systems and the simulation procedure are presented. In section III.A, the structural properties of all four systems are examined, while in section III.B the dynamics of the bound layer is compared with that of the nonbound polymer fraction at different temperatures and different polymer/graphene interfaces. In section IV, the key results of this work are summarized.

II. SIMULATION DETAILS

The simulated polymer nanocomposites were comprised by two different polymer matrices, namely PAA and PS, with the inclusion of different nanosheets, i.e., GP and GO.[5,6] Both nanographene flakes are in the nanometer range and almost quadratic, with dimensions 9×9 nm^2 and 9×8.4 nm^2 for GP and GO, respectively. A single nanographene sheet is inserted in a polymer matrix, almost centered in the simulation box. In both matrices polymer chains consist of 40 monomers, which correspond to unentangled polymer systems. Systems details, concerning the number of polymer chains (N), the total number of atoms (N_a) in each system, the size of the cubic simulation box (L_{BOX}), and the weight fraction of the nanofiller in the polymer matrix (c), are presented in Table 1.

Table 1. Systems Details

systems	N	N_a	L_{BOX} (nm)	c (wt %)
PAAGP	1300	473146	18	0.8
PAAGO	1300	479231	18	1.0
PSGP	1485	474204	22	0.5
PSGO	1485	480289	22	0.6

The filler content in all systems did not exceed 1 wt %.[5,6] Four combinations of polymer nanocomposites were constructed, as shown in Figure 1, which were labeled as (a) PAAGP, (b) PAAGO, (c) PSGP, and (d) PSGO.

To allow for an explicit representation of hydrogen-bonded-capable atomic pairs, we adopted an all-atom structure for PAA.[29,55] However, for PS where $\pi-\pi$ interactions play the most important role in the interactions with graphene-based fillers, a united atom (UA) description was used.[12,77] For the fully atomistic models, the MD runs were performed by using a time step of 1 fs, while for the UA models a time step of 2 fs was utilized. The energetic description of the PAA and GO systems[29,55] was based on the AMBER force field,[78,79] while the charge assignment on a PAA chain was based on the Gasteiger method.[80] The GO nanosheet was characterized by a carbon-to-oxygen atom ratio of 5:1 and a hydroxyl-to-epoxy group ratio of 3:2 approximately.[30,55,81] Partial charges for the GO were assigned as described in a previous work.[81] An equal number of the two different oxidized groups covered both sides of the flake (Figure S1 of the Supporting Information).

https://dx.doi.org/10.1021/acs.macromol.0c01040
Macromolecules 2020, 53, 6190−6203

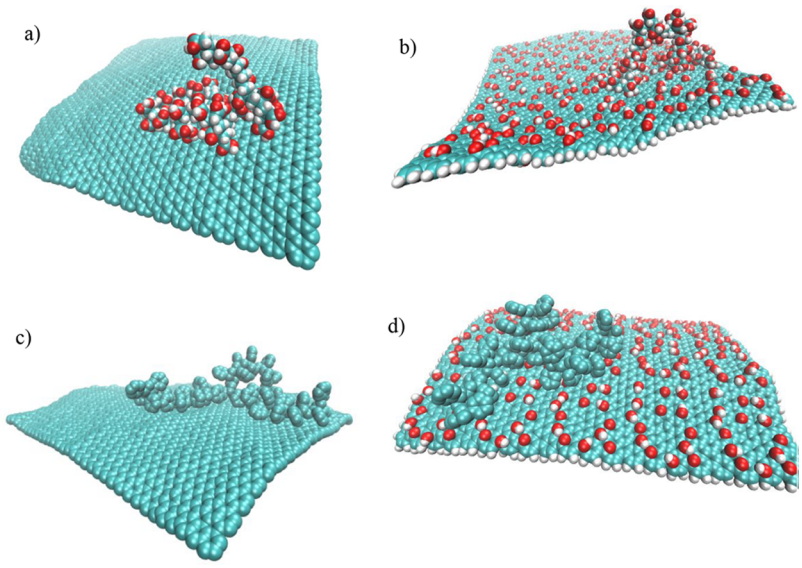

Figure 1. Snapshots of an adsorbed chain on GP and GO nanosheets at the four studied systems: (a) PAAGP at 650 K, (b) PAAGO at 650 K, (c) PSGP at 600 K, and (d) PSGO at 600 K. Beads colored in cyan, red, and white represent carbon, oxygen, and hydrogen atoms, respectively. The rest of the chains in the respective boxes are omitted for clarity.

To describe the interactions between the chemical species in PS systems, we have used the united-atom model of the TraPPE force field.[12,77,82] The specific UA PS model was found to describe accurately the structure and the thermodynamics of PS bulk chains. In addition, it was found to slightly overestimate the diffusion coefficient of bulk PS.[83,84] However, since the main goal of our current work is to provide a detailed examination of the dynamics of the bound layer, in comparison to the bulk one, we expect that the above possible differences, when compared against experimental data, are not critical. Moreover, the parameters for the nonbonded interactions of the pristine graphene carbons were taken from a potential used for graphite.[85] For the polymer/graphene interactions, the Lorentz−Berthelot rules were used.[12]

All simulations were performed with the Gromacs package,[86] in the isothermal−isobaric (NPT) ensemble, by using the velocity-rescale thermostat[87] and the Berendsen barostat.[88] All systems were first equilibrated for at least 100 ns (depending on temperature), while the production runs extended to several hundreds of nanoseconds, reaching 0.5 μs at the lowest temperature examined. The PAA-based systems were examined at 500, 550, 600, and 650 K, while the PS-based analogues at 450, 500, 550, and 600 K. For comparison purposes, the corresponding bulk polymers (PS and PAA systems at all respective temperatures) were also simulated and used as reference systems. The choice of the temperatures examined was based on a requirement that the lowest temperature value would be ∼100 K above the glass transition temperature (T_g) of the respective bulk polymers. The T_g temperatures for the pristine polymers are around 412 K for PAA[29] and 360 K for PS[12] for the molecular weights examined.

III. RESULTS AND DISCUSSION

Figure 1 presents typical adsorbed chain conformations in all four systems. Snapshots including all polymer chains are presented in Figure S2 for the PSGO and PAAGP systems. Compared to previous MD simulation studies,[55,89,90] larger systems, in terms of both number of polymer atoms and nanofiller dimensions, are studied here. The area of the nanosheet and the degree of loading of the graphene filler used in this study allow the study of polymer structural and dynamical properties under spatial confinement conditions similar to those realized in experimental works.[5,6,91] In addition, the wide temperature range examined allows for the investigation of possible structural/dynamic transitions related to the bound polymeric layer. The models examined in the present effort ensure a well-defined bound layer as well as a wide bulk region, avoiding at the same time possible finite size effects.[77]

In the case of GP, conformational transitions are present, manifesting a dynamic behavior known also as rippling or wrinkling.[92−94] In addition, GO was found to exhibit a higher tendency for curvature compared to GP.[22,62] The distribution of functional groups' charges may lead to such long-lasting curvature effects.[93,95,96]

III.A. Structural Properties. In the following, analysis of structural/conformational properties as a function of the distance from the nanographene sheet is presented. For this purpose, a series of layers parallel to the graphene flake are defined. The coordination system for the layer analysis, at each time (t), is based on the eigenvectors of the radius of gyration (R_g) tensor of the nanosheet.[22] The gyration tensor (S_{ij}) is defined based on the distance of each atom (k) from the Center of Mass (CM) of the molecule with mass m_{tot}, weighted with the mass of each atom (m_k), as[97]

$$S_{ij} = \frac{1}{m_{\text{tot}}} \sum_{k=1}^{N} m_k (r_i^{(k)} - r_i^{(\text{CM})})(r_j^{(k)} - r_j^{(\text{CM})}); \quad S = \begin{bmatrix} S_{xx} & S_{xy} & S_{xz} \\ S_{yx} & S_{yy} & S_{yz} \\ S_{zx} & S_{zy} & S_{zz} \end{bmatrix} \tag{1}$$

In this analysis, only moieties (polymer atoms or CMs of chains) whose projection in the x, y axes lie within the central 80% of the average dimensions of the nanosheet in these directions are taken into account. In this way edge effects are

https://dx.doi.org/10.1021/acs.macromol.0c01040
Macromolecules 2020, 53, 6190−6203

avoided,[13] while the tangent *xy*-plane describes more efficiently the area around the CM of the nanosheet (reduced curvature).

Figure 2 portrays the density profiles for all systems at the examined temperatures. All distances are measured with respect to a plane defined by two of the principal axes of the flake's gyration tensor (the ones that lie almost parallel to the flake and goes through the CM of the nanosheet). Henceforth, this plane will be considered as the nanosheet plane. The density values were averaged over both sides of the sheet. The binning was based on a layer width of 0.5 Å thickness, while atoms with coordinate's projections at the edges of the nanosheet are not considered in the analysis. In case that the entire nanosheet surface had been taken into account, the height of the peaks in density fluctuations (especially of the first peak) in all PAA and PS systems would have been moderately reduced. In the main graphs the *y*-axis presents densities normalized to those of the respective bulk polymer, while in the insets the mass density profiles are displayed. It is shown that the density fluctuations persist until a distance of about 20 Å, whereas for longer distances the respective bulk values are attained.

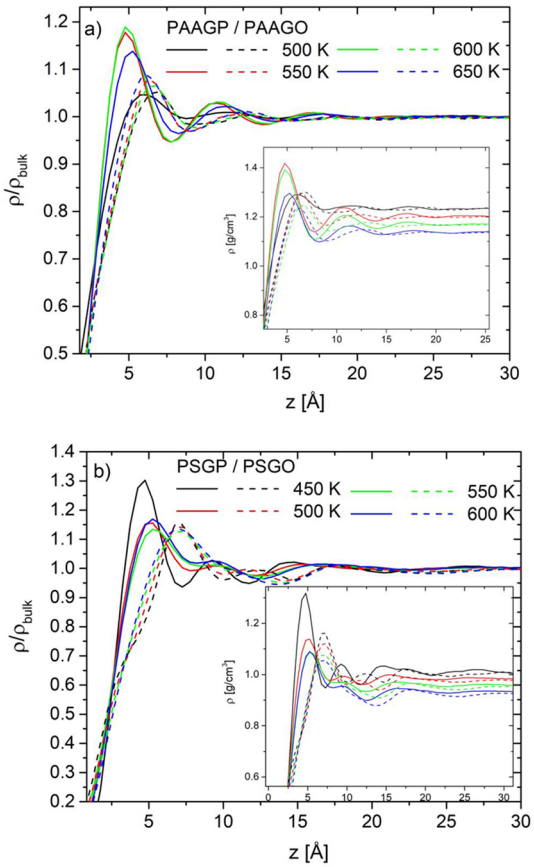

Figure 2. Normalized density profiles along a direction normal to the nanosheet plane for (a) PAAGP and PAAGO systems and (b) PSGP and PSGO systems. The mass density profiles are shown in the respective insets. The solid lines correspond to GP-based and the dashed lines to GO-based systems.

Although the rippling of the diffusing nanosheet[92] may slightly affect the density profiles close to the surface, qualitative information concerning the density fluctuations on the surface can be extracted. In the PAAGP systems, a peak is observed at a distance of almost 5 Å from the GP, which tends to become lower in amplitude and broader as the temperature drops. The latter is followed by a minimum at a distance of about 8 Å. In the entire interval, almost three peaks are observed. In the case of the PAAGO systems, the locations of all peaks are shifted at slightly longer distances with respect to the defined plane of the nanosheet. This can be accounted for by the higher roughness of the GO due to the presence of hydroxyl and epoxy groups. For the same reason the height of the first peak appears lower in the case of GO, since in the first layers, close to the nanosheet, the hydrophilic groups of the GO inhibit a higher concentration of polymer mass. Similar characteristics were found in a recent MD simulation study in poly(methyl methacrylate)/GP/GO nanocomposites,[62] where it was shown that the distribution of monomers based on the minimum distance from the surface depicts an analogous first peak height in both nanosheets. For all PAA systems, the first maximum in the normalized density profiles tends to decrease in height as the temperature drops, indicating that at the low temperature limit the density on the nanosheet and that in the bulk converge. The adhesion tension related to such behavior has been shown[15] to follow a quadratic temperature dependence.

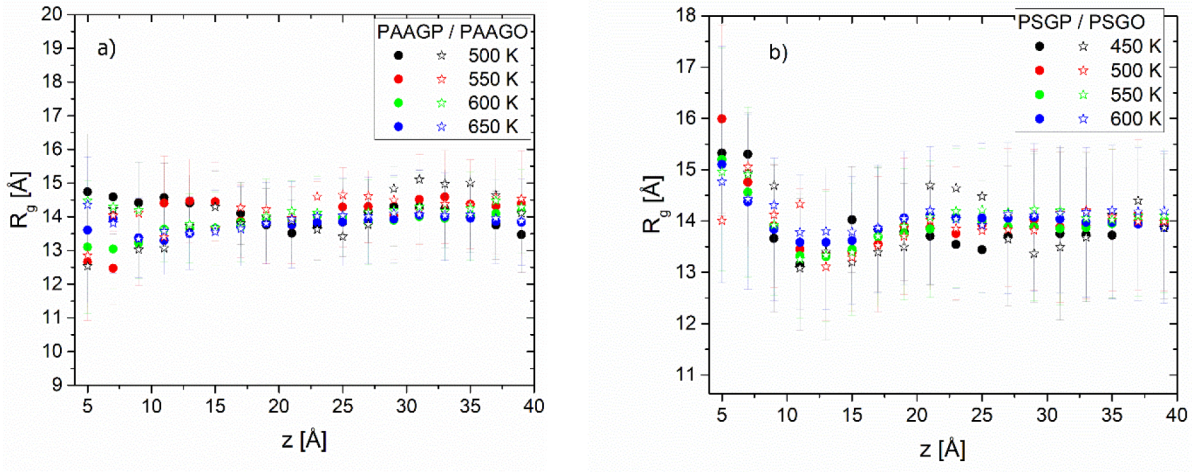

Figure 3. Profiles of the radius of gyration along a direction normal to the GP or to the GO flake for (a) the PAA and (b) the PS systems.

https://dx.doi.org/10.1021/acs.macromol.0c01040
Macromolecules 2020, 53, 6190−6203

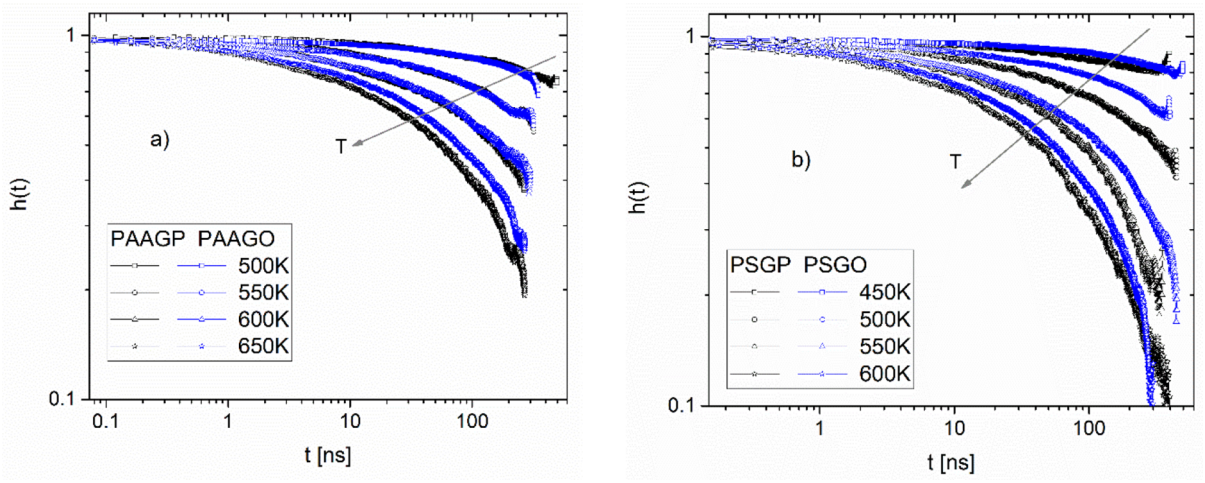

Figure 4. Desorption ACFs for (a) the PAA- and (b) PS-based systems. The adsorption state is defined based on layer0. Arrows indicate the direction of the increase in temperature.

For the PS-based systems, as shown in Figure 2b, similar trends with those noted in the PAA systems are observed, concerning the magnitude of the density fluctuations. Nevertheless, it is worth noticing that in the PSGP systems the first peak in the normalized density profiles increases as temperature drops. This behavior can be attributed to the $\pi-\pi$ interactions between the phenyl ring and the graphene sheet, which induces an increased orientation.[77] This is more pronounced at 450 K and is accompanied by more intense fluctuations in the region of 7−20 Å.

In addition, the orientation of the polymer chains on the GP and GO nanosheets is examined. Based on the second-order Legendre polynomial (P_2) of the vectors, corresponding to the lowest and highest eigenvalues of the gyration tensor, it is indicated for PS (Figure S3) a departure from the random orientation state, at distances between 0 and 20 Å. Close to the surface of the nanosheet, a preferential parallel orientation of the chains is detected. For the PSGP system, at 450 K this is more pronounced, as the values of 1.0 and −0.5 for the eigenvectors of the lowest and highest eigenvalues indicate ordered chain configurations. A typical snapshot of a PS chain, with high orientational order parallel to the surface, at 450 K, is shown in Figure S4a. An analogous behavior close to the nanosheet is observed for the PAA systems (Figure S5) as well.

It should be noted here that in the analysis regarding the dynamics of the bound polymer (presented in section III.B), the first peak of the density profile is considered as a signature for the localization of atoms; therefore, the adsorbed state is taken to extent until its first minimum.[55,98] As shown in Figure 2, this is located at a distance between 8 and 10 Å from the nanosheet.[13,29,71,89,90] Because in all systems the width of the first peak is close to 5 Å, an atom is considered as adsorbed when the minimum distance from every atom of the nanosheet is less than or equal to this value. This defines the adsorption criterion utilized in the analysis to follow. For example, in the snapshots shown in Figure 1, all chains are at least 40% adsorbed.

In Figure 3, R_g profiles in a direction normal to the nanosheet are presented for all four systems at the studied temperatures. The molecular weights (MW) of the PAA and PS chains were chosen in a manner that the two polymers assume similar R_g values in bulk (∼14 Å). In this way in all four systems the ratio of polymer dimensions to the nanosheet dimensions is kept constant, facilitating thus the study of the effect of the different adhesion affinity in the adsorbed-polymer properties at the polymer/filler interface.

In the case of the PAA systems, for both GP and GO nanofillers, chain dimensions are not significantly affected by the adsorption. Particularly for the PAAGP system at high temperatures, even a tendency for reduced dimensions can be observed, which is an indication of weak adhesion.[99] It must be noted that although in our analysis an effort was made to reduce the nanosheet edge effects, instances of chains adsorbed by both sides of the nanosheet can still be present in all systems. These chain configurations lead to the detection of polymer CMs at distances (vertical projection) even closer than 2 Å from the nanosheet. Such an example in the case of the PAAGO system is provided in Figure S6.

However, the R_g values of PS close to the GP and GO nanosheets, combined with the order parameter profile, indicate slightly more extended conformations, implying a more efficient packing of the polymer close to the filler's surface. In the PSGP system an almost 10% increase in the average dimensions of the PS coil close to the interface is observed.

III.B. Dynamical Properties. *Desorption Dynamics.* In this section the tendency for adhesion of the polymer chains on the surface of nanographene is studied, and the formation of a bound layer is examined. In the layer analysis below, the adsorbed layer (layer0) represents distances from 0 to 5 Å from the surface of the nanosheet, the next layer (layer1) involves distances between 5 and 15 Å, and the bulk layer corresponds to distances beyond 30 Å. The definition of each layer is based on the minimum distance from the atoms of the nanosheet, following thus the curvature of the latter.[13] This means that atoms are distributed into layers according to their actual position with respect to the entire GP or GO sheet.

Chain desorption dynamics from the adsorbed layer can be studied by using the following correlation function:[30]

$$h(t) = \frac{\langle g(t)g(0)\rangle}{\langle g^2\rangle} \tag{2}$$

where $g(t)$ takes the value of 1 if at least one atom of the chain satisfies the adsorption criterion at time t and 0 otherwise. $\langle\ \rangle$ denotes statistical averaging over all chains and time origins.

https://dx.doi.org/10.1021/acs.macromol.0c01040
Macromolecules 2020, 53, 6190−6203

Because in both the glassy and amorphous regions the segmental relaxation of the polymers is described by stretched exponential functions,[100−102] estimation/extrapolation regarding the relaxation times can be performed by fitting the correlation spectra to the mKKW function:[103]

$$P(t) = a_1 \exp\left[-\frac{t}{\tau_1}\right] + (1 - a_1) \exp\left[-\left(\frac{t}{\tau_2}\right)^{\beta}\right] \quad (3)$$

In eq 3, α_1 represents the fraction of fast librational motions that are described by a simple exponential and a characteristic time τ_1, while the rest of the relaxational motions are described by a stretched exponential (β parameter) and a characteristic time τ_2.[101] The mean decorrelation time, τ_c, can thus be calculated by the expression $\tau_c = \alpha_1\tau_1 + (1 - \alpha_1)\left(\frac{\tau_2}{\beta}\right)\Gamma\left(\frac{1}{\beta}\right)$, where Γ is the Gamma function.

Figure 4 shows the desorption curves for the examined systems. Fitting of the data with eq 3 provides a rough estimation of the decorrelation times (τ_c). In PAA systems, at 650 K the relaxation times amount to 215 and 276 ns for PAAGP and PAAGO systems, respectively. At lower temperatures desorption curves exhibit analogous behavior for systems of both fillers. The desorption times τ_c are roughly estimated to be around 500 ns, 1 μs, and 5 μs at 600, 550, and 500 K, respectively. It must be noted that the latter times are crude approximates which serve only to provide an order of magnitude, since they correspond to time scales much longer than the simulation runs.

At the temperature value which corresponds to the same maximum distance from the T_g (i.e., 650 K for PAA and 600 K for PS), the desorption curves of Figure 4 indicate lower residence times in the adsorbed state for PS compared to PAA. Based on Figure 4b, the decorrelation times for PSGP are estimated to be around 145 ns, 210 ns, 1 μs, and 10 μs while for PSGO 150 ns, 335 ns, 1.2 μs, and 10 μs at 600, 550, 500, and 450 K, respectively. In the PSGP systems, at 450 K, even after 500 ns, as can be seen in Figure S4, a chain may remain adsorbed although the GP undergoes intense rippling.[18]

Moreover, it was found that the estimated desorption times in all systems are much larger than the maximum relaxation times of the polymer chains in bulk, as presented in Table 2.[12,29,66] The respective relaxation curves, as shown in Figure S7, correspond to the first-order Legendre polynomial of the end-to-end vector ($P_1(t) = \langle \vec{e}(t)\cdot\vec{e}(0)\rangle$, with $\vec{e}$ being the unit vector). At the lowest temperature, after 500 ns the values of 0.4 and 0.2 are reached for the bulk PAA and PS system, respectively. In the same time interval, the desorption curves (Figure 4) depict the values of 0.7 and 0.8 for the PAA and PS system, respectively. The observed behavior implies that in both PAA and PS systems at 100 K above T_g a polymer bound layer is present,[15] which is expected to affect significantly chain dynamics.

Table 2. End-to-End Vector Decorrelation Times (τ_c) Based on the ACF Curves Presented in Figure S7 and Estimated by Eq 3

bulk PAA	τ_c [ns]	bulk PS	τ_c [ns]
500 K	972 ± 100	450 K	422 ± 100
550 K	121 ± 50	500 K	74 ± 20
600 K	40 ± 5	550 K	28 ± 5
650 K	18 ± 2	600 K	14 ± 2

Polymer Dynamics Close to the Interface. To further elaborate on the conformational dynamics of the polymer chains at the bound layer, we have monitored the backbone dihedral autocorrelation function (ACF):[98]

$$P(\varphi(t)) = \frac{\langle \cos\varphi(t)\cos\varphi(0)\rangle - \langle \cos\varphi(0)^2\rangle}{\langle \cos\varphi(0)\cos\varphi(0)\rangle - \langle \cos\varphi(0)^2\rangle} \quad (4)$$

Here, $\varphi(t)$ symbolizes a backbone dihedral angle at time t. Intramolecular torsional barriers are known to be closely associated with the glassy polymer behavior,[104] and thus calculation of the torsional decorrelation times can provide information regarding the immobilization/vitrification of the restricted polymer layer close to the filler's surface. The definition of the layers is based on the minimum distance from the surface, following the nanosheet rippling. To improve statistics, leaving and reentrance of atoms in the same layer was allowed.

Figure 5 shows the ACF curves together with the fits, using eq 3, for the adsorbed layer. For clarity, in Figure S8 only the respective fitting curves are shown. It can be observed that in general the decorrelation is slower in the GO systems for both PAA and PS systems. In PAA systems, the difference between black (GP) and blue (GO) curves at intermediate times becomes more pronounced as the temperature drops. At the lowest temperatures studied, the ACF curves reach the same value of 0.2 at 100 and 200 ns in PAAGP and PAAGO systems, respectively. It can also be observed that in the PAAGP systems the curves exhibit stronger statistical fluctuations. This is an indication that the PAA backbones near GP stay for shorter times confined within layer0 compared to the behavior observed in the PAAGO systems.

An analogous enhanced-noise/poor-statistics effect is obvious for the PS-based systems in layer0 of both GP and GO. It must be noticed that PS becomes physically adsorbed on the surface (Figure S4) mostly through the phenyl ring;[77] thus, the probability of the backbone to lay within the adsorbed layer of 5 Å thickness is lower compared to that for PAA. At 600 K and at intermediate times, the fitting renders slightly faster dynamics for the PSGO compared to the PSGP system (Figure 5b). At 450 K, after almost 400 ns, the ACFs for both PSGP and PSGO reach values close to 0.3. Almost 100 K above the calorimetric T_g of the bulk polymers, both PAA and PS systems indicate a behavior consistent with the presence of an immobilized bound layer, which is expressed through the absence of decorrelation of the backbone dihedral ACFs within a time window of almost 0.5 μs.

The effect of the immobilization of the bound layer on the dynamics of the next to the adsorbed layer (layer1) is examined in Figure 6. In contrast to Figure 5, the GO systems (blue curves) exhibit slightly faster dynamics, at short and intermediate times, in both polymer systems compared to their GP analogues (black lines). In PAA systems (Figure 6a), where the statistics is better, it can be clearly observed that the different adhesion properties of the two polymers, which affect the dynamics of the bound layer, are smeared out in layer1. At the lowest examined temperature (T = 500 K), the ACFs describing the PAAGP and PAAGO systems are practically indistinguishable.

The same trend is also present in the PS-based systems (Figure 6b). Because a chain with a characteristic dimension of

https://dx.doi.org/10.1021/acs.macromol.0c01040
Macromolecules 2020, 53, 6190−6203

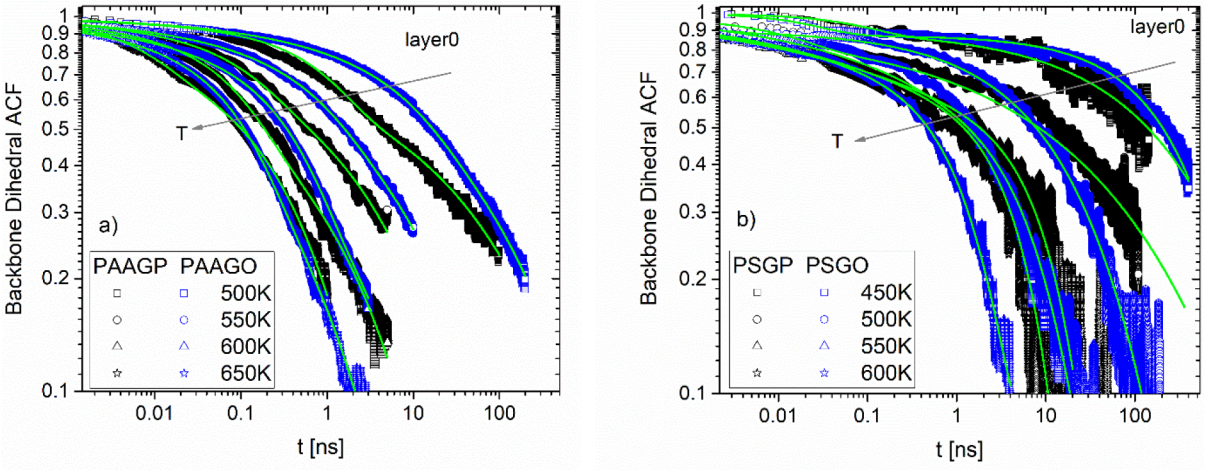

Figure 5. Backbone dihedral ACFs for (a) the PAA and (b) PS systems in layer0. The green solid lines represent the respective mKWW (eq 3) fits. Arrows denote the direction of the increase in temperature.

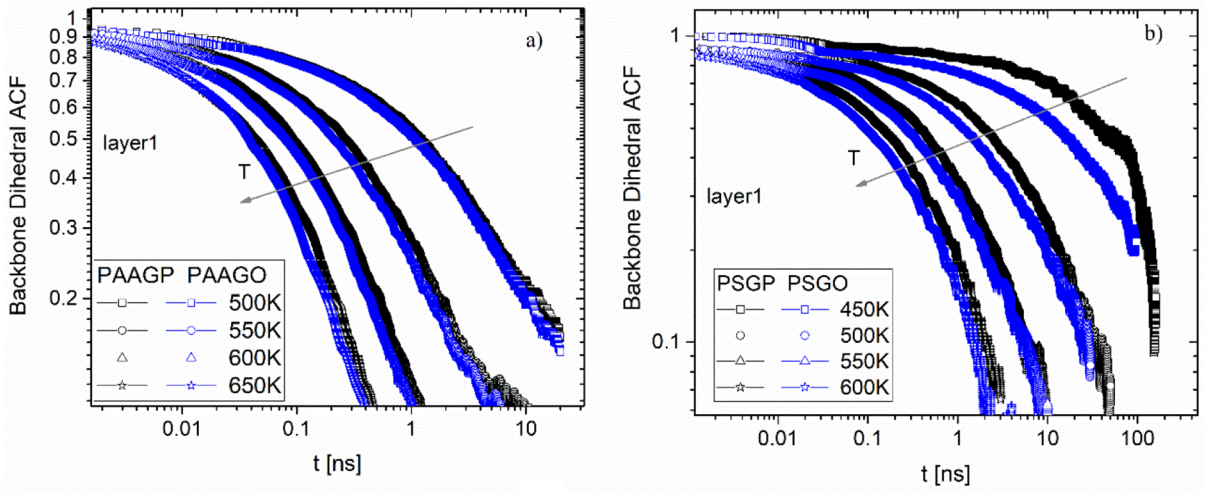

Figure 6. Backbone dihedral ACFs for (a) the PAA and (b) PS systems in layer1. Arrows denote the direction of the increase in temperature.

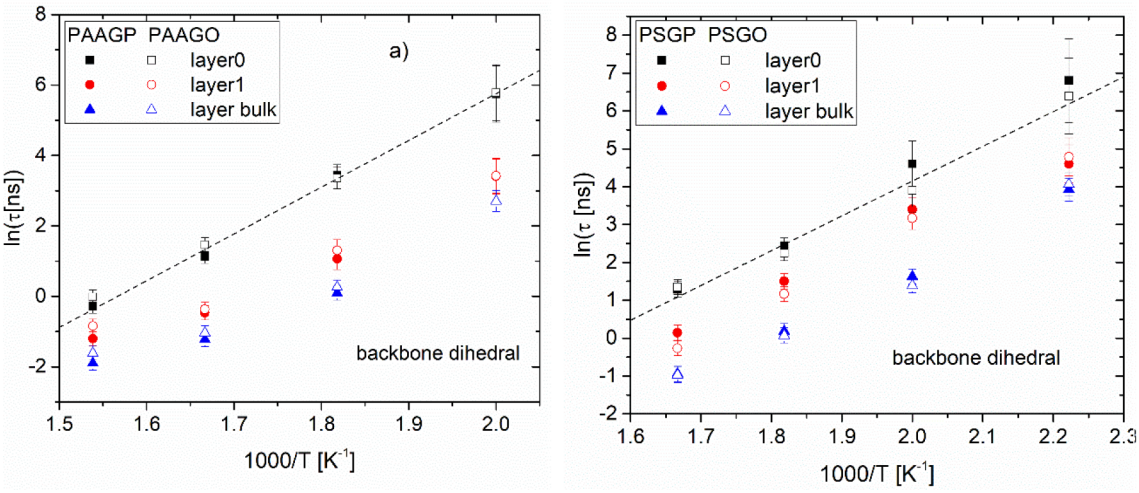

Figure 7. Arrhenius plots of the decorrelation times of the backbone dihedral ACFs for the (a) PAA and (b) PS systems in layer0, layer1, and bulk.

$R_g \sim 14$ Å may participate in both layers adjacent to the surface (i.e., layer0 and layer1), it can be envisioned that a single adsorbed macromolecule may experience heterogeneous dynamics across its length.[61,105] The restricted dynamics of the bound layer is compensated by faster dynamics in the layer adjacent to it.

To quantify the differences observed in the relaxational characteristics of the spectra presented in Figures 5 and 6,

https://dx.doi.org/10.1021/acs.macromol.0c01040
Macromolecules 2020, 53, 6190−6203

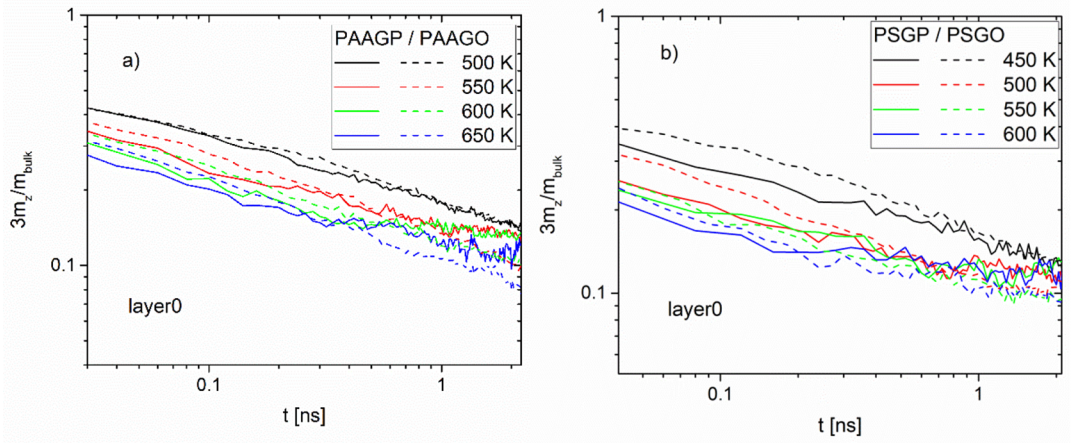

Figure 8. Time evolution of the z-mobility ratios in the direction normal to the nanosheet in layer0 for the (a) PAA systems and (b) PS systems.

decorrelation times (τ_c) calculated by means of eq 3 are presented in Figure 7. The estimated relaxation times are plotted in logarithmic scale so that any deviations from the Arrhenius behavior can be readily identified. We note that the estimation of the relaxation times of the bound layer, especially at low temperatures, is achieved by an extrapolation based on short times, and for this reason the uncertainty in the evaluation of the decorrelation time is rather high. Figure 7 shows the decorrelation times for PAA systems for all three layers (i.e., layer0, layer1, and bulk). A differentiation between the dynamics of layer0 and layer1 is noticed. Moreover, it can be observed that although the times correspond to the bulk and to layer1 follow the anticipated VFT temperature dependence,[42] the dependence describing layer0 seems to be Arrhenius-like.[17,36,41,48,50,55] This appears to be independent of the adhesion properties of the polymer.

In the case of the PSGP-based systems, the Arrhenius-like behavior has been confirmed experimentally in a recent dielectric study,[17] and our simulation seems to agree with this tendency (Figure 7b). A stronger transition is also in agreement with the experimentally confirmed absence of a heat capacity step for the bound layer in such nanocomposite systems.[15,17] Nevertheless, for the PSGP systems, at 450 K, it is possible that an even more dramatic immobilization (possible first-order transition to a liquid crystalline phase) could be present. In such a case layer1 could follow the same bound layer characteristics.

In all PAA and PS systems, the behavior of τ_c, particularly at the lower temperature values, also indicates a decoupling in dynamics between layer1 and layer0. Moreover, the temperature dependence of the β parameter (eq 3) for the bound layer (depicted in Tables S1 and S2), although it takes values between 0.3 and 0.5, does not follow a clear trend. A rather broad distribution of relaxation times is suggested.

Anisotropy of Polymer Translational Motion in the Composites. The existence of a bound polymer layer affects the translational dynamics of polymer chains, inducing anisotropy in the three directions of motion. The time evolution of the atom displacement, $\Delta r(t)$, of polymer molecules provides a measure for the dynamic gradient in segmental motion across different layers parallel to the nanosheet. To quantify this, we define an effective mobility (m), which for the case of the diffusion in one dimension (e.g., in the z direction, m_z) is represented by the z component of the mean-square displacement (MSD), i.e., $m_z(t) = \mathrm{MSD}_z(t)$. In analogy, for the case of the diffusion in a plane, the mobility quantity (m_{xy}) can be defined as the sum of the x and y components of the mean-square displacement, i.e., $m_{xy}(t) = (\mathrm{MSD}_x(t) + \mathrm{MSD}_y(t))$. Finally for isotropic diffusion (bulk systems), the effective mobility (m_{bulk}), is the sum over the x, y, and z components of the mean-square displacement to yield $m_{\mathrm{bulk}}(t) = (\mathrm{MSD}_x(t) + \mathrm{MSD}_y(t) + \mathrm{MSD}_z(t))$.

Thus, the ratios $\frac{3m_{xy}(t)}{2m_{\mathrm{bulk}}(t)}$ and $\frac{3m_z(t)}{m_{\mathrm{bulk}}(t)}$ can provide a measure for the evolution of the decoupling (at short times) between the dynamics in confined layers and the bulk dynamics.[13,29] In case the two ratios approach unity, then no decoupling is assumed. Moreover, comparison between the two ratios may offer information regarding the anisotropic characteristics of the diffusion in each layer.

Here the layer definition is based again on the minimum distance from the surface; following the nanosheet rippling, the displacement of each atom is projected to the filler's coordination system to derive the components of the MSD in the xy-plane and the z-direction parallel and perpendicular to nanosheet, respectively. The bulk layer (i.e., far from the filler's surface) is compared with bulk polymer samples at all temperatures and shows similar behavior. An atom should stay for the entire time period in the same layer, with no reentrances allowed (considering the saving frequency of ∼1 frame every 30 ps), to be taken into account in the layer analysis.

Figure 8 presents average segmental mobility ratios for the perpendicular motion of the atoms belonging in the adsorbed layer (layer0) for both polymers. Focusing on Figure 8a, a weaker decoupling of the displacement in the z-direction from the bulk is observed (i.e., the z-mobility ratio approaches 1) as temperature drops.[13] Another observation is that at somewhat longer time scales the temperature dependence of the z-mobility ratio persists in the PAAGO systems, while it reduces in the PAAGP systems. This might be related to the affinity of PAA to form hydrogen bonds with GO, which can survive at that time scale,[30] contributing thus to the departure of the mobility of the hydrogen-bonded atoms from the bulk behavior.

The z-mobility ratio increases as the temperature drops in the PS systems as well, as depicted in Figure 8b. However, the decoupling effect appears to be stronger for the PSGP systems, compared to the PSGO, and the normalized coefficient exhibits slightly lower values at all temperatures. The presence

https://dx.doi.org/10.1021/acs.macromol.0c01040
Macromolecules 2020, 53, 6190−6203

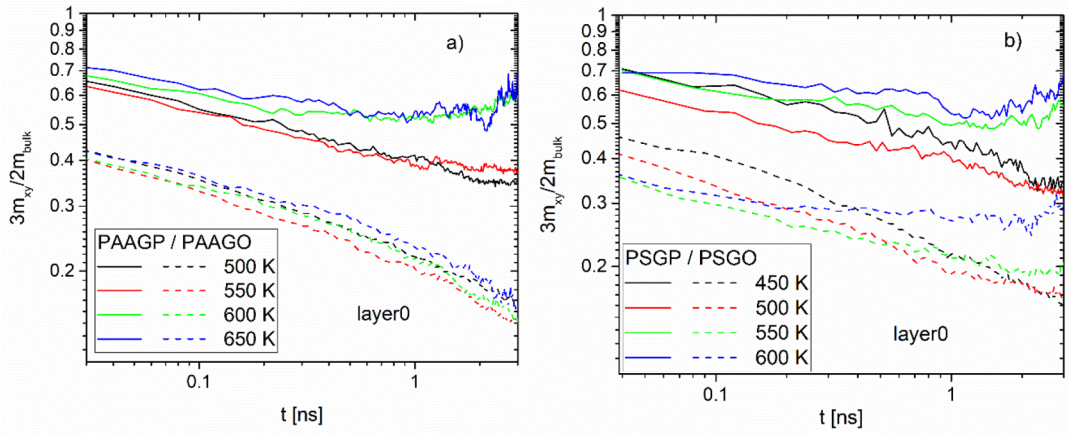

Figure 9. Time evolution of the *xy*-mobility ratio in the direction parallel to the nanosheet in layer0 for the (a) PAA systems and (b) PS systems.

of the oxygen groups in the GO sheet may inhibit the $\pi-\pi$ interactions between some of the phenyl groups of PS and the filler, affecting thus their tendency to adsorb and therefore influence the polymer's local dynamics. At longer time scales, the mobility ratios between the PSGP and the PSGO models assume similar values, in contrast to what was observed for the PAAGO system, presumably due to the absence of hydrogen-bond formation in the PS-based systems.

Figure 9 shows the planar mobility ratio of atoms residing in layer0. For PAA in systems with both nanosheets (Figure 9a), as the temperature drops the degree of decoupling marginally increases. Moreover, it is shown that the mobility ratio behavior parallel to the nanosheet is markedly different between the GP and GO systems at all the examined temperatures. The planar mobility ratio appears to be considerably lower in the PAAGO systems compared to that in the PAAGP. This can be rationalized by a combined effect related to the presence of hydrogen bonding in the GO-based system as well as to the higher degree of roughness of the GO sheet, which is known to slow down translational dynamics.[99,106]

Figure 9b, portraying the behavior of the PS-based systems, shows in general a behavior similar to that of the PAA-based composites, but with some quantitative differences. Namely, the mobility ratios in the PSGO system show a somewhat stronger temperature dependence and slightly higher ratios at lower temperatures compared to their PAAGO analogues. This might be related to the absence of hydrogen bonding in the PSGO system, which allows a less restricted planar translational motion that can be more easily affected by changes in temperature.

The picture emerging from both PAA and PS systems, at all temperatures, supports the idea that in the absence of increased nanoroughness (i.e., as in the GP nanosheet) the mobility suppression in the *z*-direction is accompanied by a less suppressed mobility in the *xy*-plane, implying a strongly anisotropic diffusion. Similar results have also been observed for the diffusion of small molecules in the calcite surface[107] and macromolecules in the graphite surface.[12,65,73,104] The higher the suppression of the displacement in the *z*-direction, the higher the mobility in the *xy*-plane, resulting in an average mobility ratio closer to 1.[107] The ability of smooth surfaces to retain part of the translational entropy, at high enough temperatures, in the *xy*-plane could in a thermodynamic way explain the increased first peak in the density profile in the GP nanosheets. In the case of immobilization/ordering (at a lower temperature) of the bound layer on the nanosheet, the entropy reduction on the GP is expected to be higher than the one on the GO.[99] On a DSC thermogram, such behavior of abrupt reduction in the entropy could be manifested as a crystallization peak.[8,17,18]

Nevertheless, a higher degree of roughness, as introduced by the hydroxyl and epoxy groups of GO, results in a more isotropic ($2m_z/m_{xy} \approx 1$) diffusion compared to that in the GP-based systems. The average mobility ratios (parallel and perpendicular to the surface) are lower in these systems, indicating stronger decoupling effects. Because desorption of the atoms, when no layer reentrance is allowed, results in noisier curves, it is clear that the PAAGO atoms remain for longer times adsorbed, exhibiting smoother m_{xy} curves at all temperatures. Compared to an analysis that would allow reentrance of the atoms in the layer, only contributions from large displacements at longer times (>1 ns) are missed.[13]

At the layer next to the adsorbed (layer1, width of 10 Å) polymer atoms move faster. The normalized planar mobility ratio assumes values higher than those in layer0, as shown in Figure S9. These values lie within the same range for both GP- and GO-based systems. The coefficient m_z (data not shown here) indicates also a more isotropic diffusion. In other words, it appears that the adsorbed layer (layer0) provides a kind of shielding/coating to the next layer from the effects of surface roughness and hydrogen bonding (where present), as far as it concerns polymer dynamics close to the nanosheet.[15,39,108]

Dynamic Heterogeneity Close to the Surface of the Nanosheet. To elaborate more on the degree of dynamic heterogeneity (cooperativity in diffusion) close to the surface of the nanofillers, one can monitor the non-Gaussian parameter (NGP), α_2, defined as

$$a_2(t) = \frac{3\langle \Delta r(t)^4 \rangle}{5\langle \Delta r(t)^2 \rangle^2} - 1 \quad (5)$$

where $\Delta r(t)$ denotes the mean-squared displacement of the atoms (which can be calculated in different directions) at time t and the brackets symbolize time and ensemble average. After time t, if all the atoms have traveled the same distance, α_2 takes a value of −0.4. In Brownian motion, α_2 takes a value of 0, while in cases where the displacements are not Gaussian distributed, values greater than 0 appear.

In Figure S10, it is shown that the α_2 parameter indicates a similar degree of heterogeneity for both pristine PAA and PS

https://dx.doi.org/10.1021/acs.macromol.0c01040
Macromolecules 2020, 53, 6190−6203

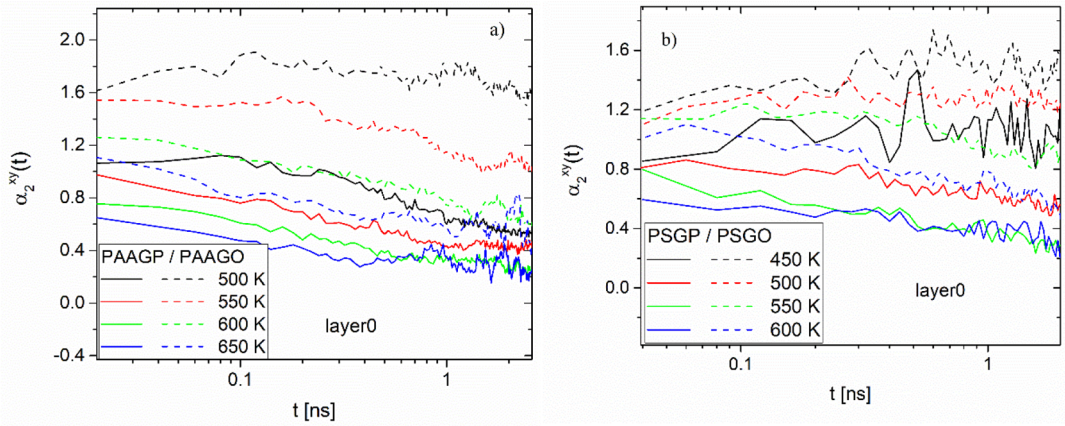

Figure 10. Non-Gaussian parameter (α_2) of the atomic displacements parallel to the nanosheet (*xy*-plane) in layer0 for the (a) PAA systems and (b) PS systems.

systems at the examined temperatures. This suggests that in both polymer systems the distance from T_g at the corresponding temperatures is similar. At high temperatures and short times (~50 ps) the polymer bulk dynamics assume rather low α_2 values, close to 0.5. The same quantity at the lowest temperature reaches more than twice the value observed at high temperature, i.e., close to 1.2. Therefore, the temperature range examined covers the transition regime where bulk polymer dynamics change from almost homogeneous to strongly heterogeneous.

The behavior of the NGP of polymer atoms close to the nanosheet, moving parallel to it (i.e., *xy*), at all studied temperatures in the composite systems is shown in Figure 10. The definition of layers is the same as that in the study of the MSD discussed earlier. Based on the coordination system, the displacement is projected on the *xy*-plane parallel to the nanosheet. In all models, the NGP drops when temperature increases, as does the distance from T_g. It is also evident that for both the PAA- and PS-based systems the presence of GO induces a higher degree of heterogeneity compared to their GP analogues. Although close to the surface of GO the diffusion (in all three directions) is more isotropic, the dynamic heterogeneity (NGP) in the *xy*-plane is higher.

Remarkably, diffusional motion close to GP not only exhibits lower α_2 values but also the degree of dynamic heterogeneity in the *xy*-plane in the composite is very close to that corresponding to the bulk polymers at the same temperature values, which is not the case for the GO-based systems. Even at longer time scales (~1 ns), the NGP values in the GO systems are higher for both PAA and PS systems compared to the respective bulk polymers at the corresponding temperatures. The bound layer dynamics on both nanosheets does not exhibit a suppression of the heterogeneity compared to the bulk. The observed behavior implies that an experimental technique capable of probing local relaxational dynamics close to the nanofiller would have detected broader spectra in the GO composites.

The overall analysis is consistent with the formation of a dynamically arrested interfacial polymer layer at a temperature almost 100 K above the bulk calorimetric T_g. This notion appears to be independent of the nanofiller roughness. Information about the global chain dynamics and the structure of the adsorbed layer will be presented in a future work.

IV. CONCLUSIONS

In the current work we have presented an MD simulation study focusing on the bound polymer layer on GP and GO nanosheets. Two polymer matrices have been used, namely PAA and PS. The two different nanosheets bear different degrees of surface roughness and exhibit different affinities with the examined polymeric chains. The choice of polar and hydrogen-bonding-capable PAA and nonpolar but $\pi-\pi$ interaction active PS allows the examination of restricted polymer dynamics under different conditions of adhesion with the nanofiller. To eliminate possible size effects in the presence of nanometer-sized graphene and graphene oxide sheets and to accomplish an equilibrium of the adsorbed layer with the bulk fraction, large systems, of the order of 500×10^3 atoms, were studied. The examined temperature range covered temperatures between 100 and 250 K above T_g for both polymers, allowing the observation of the transition between an immobilized layer close to the filler's surface to a more mobile dynamic state.

Density profiles indicate a bound layer width of almost 5 Å. This length is used in the layer analysis parallel to the nanoflake. In the PAAGO system, lower densities were detected close to the nanosheet compared to those observed in the PAAGP system. A similar trend was also noticed in the PS systems, indicating that the increased surface roughness of GO leads to lower polymer densities close to the surface.

Concerning the dynamics of the bound layer, the key results of this study can be summarized as follows: (1) The desorption dynamics and the backbone torsional relaxation indicated that for the polymers studied, at a temperature ~100 K above their corresponding bulk T_g, a layer with suppressed mobility is formed close to the examined nanofillers. (2) The experimentally detected "stronger" transition/Arrhenius-like behavior, close to the fillers surface, was observed in all the systems, despite the differences in the filler's nanoroughness and in the relative affinity between the polymer and the GP-based flake. (3) A faster, less heterogeneous, and more anisotropic diffusional motion was present in the lower roughness GP-based systems compared to the GO-based systems. (4) An increased dynamic heterogeneity of the bound layer compared to the bulk one was detected for all systems. (5) The MSD on the layer adjacent to the adsorbed one exhibited isotropic characteristics for all systems, independent

https://dx.doi.org/10.1021/acs.macromol.0c01040
Macromolecules 2020, 53, 6190−6203

of the degree of the filler's roughness or the presence of specific interactions.

On the basis of the above, it can be concluded that polymer chains experience different dynamic regimes close to the nanosheet, with the adsorbed layer providing a shielding effect to the adjacent layer. In the vicinity of the surface, the cooperativity is expressed as a strong dynamic decoupling between the two layers.

■ ASSOCIATED CONTENT

Supporting Information

The Supporting Information is available free of charge at https://pubs.acs.org/doi/10.1021/acs.macromol.0c01040.

Figure S1: snapshots of the initial GO configuration; Figure S2: a snapshot of the whole PSGO and PAAGP systems; Figure S3: the order parameter of PS chains based on the eigenvectors; Figure S4: the evolution of the adsorbed PS chain on GP; Figure S5: the order parameter of PAA chains based on the eigenvectors; Figure S6: a snapshot of PAA chain adsorbed by both sides of the GO flake; Figure S7: the end-to-end vector decorrelation functions for bulk PAA and PS; Figure S8: the mKWW fittings of torsion ACFs for the bound layer of PAA and PS; Tables S1 and S2: β-parameters of the mKWW fittings; Figure S9: the time evolution of the normalized planar mobility ratios in layer1; Figure S10: the bulk non-Gaussian parameters for both PAA and PS (PDF)

■ AUTHOR INFORMATION

Corresponding Authors

Georgios Kritikos − *Laboratory of Physical Chemistry, Department of Chemical Engineering, Aristotle University of Thessaloniki, Thessaloniki 54124, Greece;* orcid.org/0000-0003-2579-6597; Email: kritikgio@cheng.auth.gr

Anastassia N. Rissanou − *Institute of Applied and Computational Mathematics, Foundation for Research and Technology - Hellas, Heraklion GR-71110, Greece;* orcid.org/0000-0003-1393-7639; Email: rissanou@iesl.forth.gr

Authors

Vagelis Harmandaris − *Institute of Applied and Computational Mathematics, Foundation for Research and Technology - Hellas, Heraklion GR-71110, Greece; Department of Mathematics and Applied Mathematics, University of Crete, Heraklion GR-71110, Greece; Computation-based Science and Technology Research Center, The Cyprus Institute, Nicosia 2121, Cyprus;* orcid.org/0000-0002-9613-7639

Kostas Karatasos − *Laboratory of Physical Chemistry, Department of Chemical Engineering, Aristotle University of Thessaloniki, Thessaloniki 54124, Greece;* orcid.org/0000-0001-7431-5177

Complete contact information is available at: https://pubs.acs.org/10.1021/acs.macromol.0c01040

Notes

The authors declare no competing financial interest.

■ ACKNOWLEDGMENTS

This work was supported by computational time granted from the Greek Research & Technology Network (GRNET) in the National HPC facility—ARIS—under project ID pr003015-NANOGRAPH.

■ REFERENCES

(1) Novoselov, K. S.; Geim, A. K.; Morozov, S. V.; Jiang, D.; Zhang, Y.; Dubonos, S. V.; Grigorieva, I. V.; Firsov, A. A. Electric Field Effect in Atomically Thin Carbon Films. *Science (Washington, DC, U. S.)* **2004**, *306* (5696), 666−669.

(2) Stankovich, S.; Dikin, D. A.; Dommett, G. H. B.; Kohlhaas, K. M.; Zimney, E. J.; Stach, E. A.; Piner, R. D.; Nguyen, S. T.; Ruoff, R. S. Graphene-Based Composite Materials. *Nature* **2006**, *442* (7100), 282−286.

(3) Ramanathan, T.; Abdala, A. A.; Stankovich, S.; Dikin, D. A.; Herrera-Alonso, M.; Piner, R. D.; Adamson, D. H.; Schniepp, H. C.; Chen, X.; Ruoff, R. S.; et al. Functionalized Graphene Sheets for Polymer Nanocomposites. *Nat. Nanotechnol.* **2008**, *3* (6), 327−331.

(4) Bai, H.; Li, C.; Shi, G. Functional Composite Materials Based on Chemically Converted Graphene. *Adv. Mater.* **2011**, *23* (9), 1089−1115.

(5) Papageorgiou, D. G.; Kinloch, I. A.; Young, R. J. Mechanical Properties of Graphene and Graphene-Based Nanocomposites. *Prog. Mater. Sci.* **2017**, *90*, 75−127.

(6) Potts, J. R.; Dreyer, D. R.; Bielawski, C. W.; Ruoff, R. S. Graphene-Based Polymer Nanocomposites. *Polymer* **2011**, *52* (1), 5−25.

(7) Socoliuc, A.; Gnecco, E.; Maier, S.; Pfeiffer, O.; Baratoff, A.; Bennewitz, R.; Meyer, E. Atomic-Scale Control of Friction by Actuation of Nanometer-Sized Contacts. *Science (Washington, DC, U. S.)* **2006**, *313* (5784), 207−210.

(8) Gulde, M.; Rissanou, A. N.; Harmandaris, V.; Müller, M.; Schäfer, S.; Ropers, C.; Mueller, M.; Schäfer, S.; Ropers, C. Dynamics and Structure of Monolayer Polymer Crystallites on Graphene. *Nano Lett.* **2016**, *16* (11), 6994−7000.

(9) Kim, H.; Abdala, A. A.; MacOsko, C. W. Graphene/Polymer Nanocomposites. *Macromolecules* **2010**, *43*, 6515−6530.

(10) Skountzos, E. N.; Anastassiou, A.; Mavrantzas, V. G.; Theodorou, D. N. Determination of the Mechanical Properties of a Poly (Methyl Methacrylate) Nanocomposite with Functionalized Graphene Sheets through Detailed Atomistic Simulations. *Macromolecules* **2014**, *47* (22), 8072−8088.

(11) Napolitano, S.; Wübbenhorst, M. The Lifetime of the Deviations from Bulk Behaviour in Polymers Confined at the Nanoscale. *Nat. Commun.* **2011**, *2* (1), 260.

(12) Rissanou, A. N.; Harmandaris, V. Dynamics of Various Polymer-Graphene Interfacial Systems through Atomistic Molecular Dynamics Simulations. *Soft Matter* **2014**, *10* (16), 2876−2888.

(13) Bačová, P.; Rissanou, A. N.; Harmandaris, V. Edge-Functionalized Graphene as a Nanofiller: Molecular Dynamics Simulation Study. *Macromolecules* **2015**, *48* (24), 9024−9038.

(14) Butt, H. J.; Duran, H.; Egger, W.; Faupel, F.; Harmandaris, V.; Harms, S.; Johnston, K.; Kremer, K.; Lin, F. Y.; Lue, L.; et al. Interphase of a Polymer at a Solid Interface. *Macromolecules* **2014**, *47* (23), 8459−8465.

(15) Kritikos, G. Transition of the Bounded Polymer Layer to a Rigid Amorphous Phase: A Computational and DSC Study. *Polymer* **2014**, *55* (18), 4658−4670.

(16) Paul, D. R.; Robeson, L. M. Polymer Nanotechnology: Nanocomposites. *Polymer* **2008**, *49* (15), 3187−3204.

(17) Koutsoumpis, S.; Klonos, P.; Raftopoulos, K. N.; Papadakis, C. M.; Bikiaris, D.; Pissis, P. Morphology, Thermal Properties and Molecular Dynamics of Syndiotactic Polystyrene (s-PS) Nanocomposites with Aligned Graphene Oxide and Graphene Nanosheets. *Polymer* **2018**, *153*, 548−557.

(18) Wang, C.; Chiu, Y. C.; Huang, C. L. Electrical Percolation and Crystallization Kinetics of Semi-Crystalline Polystyrene Composites Filled with Graphene Nanosheets. *Mater. Chem. Phys.* **2015**, *164*, 206−213.

(19) Xie, Z. T.; Fu, X.; Wei, L. Y.; Luo, M. C.; Liu, Y. H.; Ling, F. W.; Huang, C.; Huang, G.; Wu, J. New Evidence Disclosed for the

Engineered Strong Interfacial Interaction of Graphene/Rubber Nanocomposites. *Polymer* **2017**, *118*, 30−39.
(20) Gong, L. X.; Pei, Y. B.; Han, Q. Y.; Zhao, L.; Wu, L.; Bin; Jiang, J. X.; Tang, L. C. Polymer Grafted Reduced Graphene Oxide Sheets for Improving Stress Transfer in Polymer Composites. *Compos. Sci. Technol.* **2016**, *134*, 144−152.
(21) Yang, G.; Liao, Z.; Yang, Z.; Tang, Z.; Guo, B. Effects of Substitution for Carbon Black with Graphene Oxide or Graphene on the Morphology and Performance of Natural Rubber/Carbon Black Composites. *J. Appl. Polym. Sci.* **2015**, *132* (15), 41832.1−41832.9.
(22) Kritikos, G.; Pant, R.; Sengupta, S.; Karatasos, K.; Venkatnathan, A.; Lyulin, A. V. Nanostructure and Dynamics of Humidified Nafion/Graphene-Oxide Composites via Molecular Dynamics Simulations. *J. Phys. Chem. C* **2018**, *122* (40), 22864−22875.
(23) Compton, O. C.; Jain, B.; Dikin, D. A.; Abouimrane, A.; Amine, K.; Nguyen, S. T. Chemically Active Reduced Graphene Oxide with Tunable C/O Ratios. *ACS Nano* **2011**, *5* (6), 4380−4391.
(24) Yu, Y. H.; Lin, Y. Y.; Lin, C. H.; Chan, C. C.; Huang, Y. C. High-Performance Polystyrene/Graphene-Based Nanocomposites with Excellent Anti-Corrosion Properties. *Polym. Chem.* **2014**, *5* (2), 535−550.
(25) Eda, G.; Chhowalla, M. Graphene-Based Composite Thin Films for Electronics. *Nano Lett.* **2009**, *9* (2), 814−818.
(26) Khodagholy, D.; Rivnay, J.; Sessolo, M.; Gurfinkel, M.; Leleux, P.; Jimison, L. H.; Stavrinidou, E.; Herve, T.; Sanaur, S.; Owens, R. M.; et al. High Transconductance Organic Electrochemical Transistors. *Nat. Commun.* **2013**, *4* (1), 2133.
(27) Kassaee, M. Z.; Motamedi, E.; Majdi, M. Magnetic Fe_3O_4-Graphene Oxide/Polystyrene: Fabrication and Characterization of a Promising Nanocomposite. *Chem. Eng. J.* **2011**, *172* (1), 540−549.
(28) Fang, M.; Wang, K.; Lu, H.; Yang, Y.; Nutt, S. Covalent Polymer Functionalization of Graphene Nanosheets and Mechanical Properties of Composites. *J. Mater. Chem.* **2009**, *19* (38), 7098−7105.
(29) Karatasos, K.; Kritikos, G. Characterization of a Graphene Oxide/Poly(Acrylic Acid) Nanocomposite by Means of Molecular Dynamics Simulations. *RSC Adv.* **2016**, *6* (111), 109267−109277.
(30) Karatasos, K.; Kritikos, G. A Microscopic View of Graphene-Oxide/Poly(Acrylic Acid) Physical Hydrogels: Effects of Polymer Charge and Graphene Oxide Loading. *Soft Matter* **2018**, *14* (4), 614−627.
(31) Zhang, W.; Shi, X.; Zhang, Y.; Gu, W.; Li, B.; Xian, Y. Synthesis of Water-Soluble Magnetic Graphene Nanocomposites for Recyclable Removal of Heavy Metal Ions. *J. Mater. Chem. A* **2013**, *1* (5), 1745−1753.
(32) Wang, L.; Wang, D.; Dong, Z.; Zhang, F.; Jin, J. Interface Chemistry Engineering for Stable Cycling of Reduced GO/SnO 2 Nanocomposites for Lithium Ion Battery. *Nano Lett.* **2013**, *13* (4), 1711−1716.
(33) Jiang, Z.; Xia, D.; Li, Y.; Li, J.; Li, Q.; Chen, M.; Huang, Y.; Besenbacher, F.; Dong, M. Facilitating the Mechanical Properties of a High-Performance PH-Sensitive Membrane by Cross-Linking Graphene Oxide and Polyacrylic Acid. *Nanotechnology* **2013**, *24* (33), 335704.
(34) Zhong, M.; Liu, Y. T.; Xie, X. M. Self-Healable, Super Tough Graphene Oxide-Poly(Acrylic Acid) Nanocomposite Hydrogels Facilitated by Dual Cross-Linking Effects through Dynamic Ionic Interactions. *J. Mater. Chem. B* **2015**, *3* (19), 4001−4008.
(35) Shen, J.; Yan, B.; Li, T.; Long, Y.; Li, N.; Ye, M. Mechanical, Thermal and Swelling Properties of Poly(Acrylic Acid)-Graphene Oxide Composite Hydrogels. *Soft Matter* **2012**, *8* (6), 1831−1836.
(36) Xu, H.; Song, Y.; Jia, E.; Zheng, Q. Dynamics Heterogeneity in Silica-Filled Nitrile Butadiene Rubber. *J. Appl. Polym. Sci.* **2018**, *135* (22), 63−67.
(37) Wood, C. D.; Chen, L.; Burkhart, C.; Putz, K. W.; Torkelson, J. M.; Brinson, L. C. Measuring Interphase Stiffening Effects in Styrene-Based Polymeric Thin Films. *Polymer* **2015**, *75*, 161−167.
(38) Hamed, G. R.; Hatfield, S. On the Role of Bound Rubber in Carbon-Black Reinforcement. *Rubber Chem. Technol.* **1989**, *62* (1), 143−156.
(39) Starr, F. W.; Douglas, J. F.; Meng, D.; Kumar, S. K. Bound Layers "Cloak" Nanoparticles in Strongly Interacting Polymer Nanocomposites. *ACS Nano* **2016**, *10* (12), 10960−10965.
(40) Song, M.; Cai, D. Graphene Functionalization: A Review. In *Polymer- Graphene Nanocomposites*; Mittal, V., Ed.; RSC Nanoscience & Nanotechnology; Royal Society of Chemistry: Cambridge, 2012; pp 1−52.
(41) Baeza, G. P.; Dessi, C.; Costanzo, S.; Zhao, D.; Gong, S.; Alegria, A.; Colby, R. H.; Rubinstein, M.; Vlassopoulos, D.; Kumar, S. K. Network Dynamics in Nanofilled Polymers. *Nat. Commun.* **2016**, *7*, 11368.
(42) Vogel, H. The Temperature Dependence Law of the Viscosity of Fluids. *Phys. Z.* **1921**, *22*, 645−646.
(43) Tammann, G.; Hesse, W. The Dependancy of Viscosity on Temperature in Hypothermic Liquids. *Z. Anorg. Allg. Chem.* **1926**, *156*, 245−257.
(44) Fulcher, G. S. Analysis of Recent Measurments of the Viscosity of Glasses. *J. Am. Ceram. Soc.* **1925**, *8* (6), 339−355.
(45) Ediger, M. D. Spatially Heterogeneous Dynamics in Supercooled Liquids. *Annu. Rev. Phys. Chem.* **2000**, *51* (1), 99−128.
(46) Adam, G.; Gibbs, J. H. On the Temperature Dependence of Cooperative Relaxation Properties in Glass-Forming Liquids. *J. Chem. Phys.* **1965**, *43* (1), 139−146.
(47) Kritikos, G. Mean Field Description of the Structural Heterogeneities in the Region of Cooperative Diffusion. *Comput. Mater. Sci.* **2020**, *179*, 109682.
(48) Anastasiadis, S. H.; Karatasos, K.; Vlachos, G.; Manias, E.; Giannelis, E. P. Nanoscopic-Confinement Effects on Local Dynamics. *Phys. Rev. Lett.* **2000**, *84* (5), 915−918.
(49) Barut, G.; Pissis, P.; Pelster, R.; Nimtz, G. Glass Transition in Liquids: Two versus Three-Dimensional Confinement. *Phys. Rev. Lett.* **1998**, *80* (16), 3543−3546.
(50) Kirst, K. U.; Kremer, F.; Litvinov, V. M. Broad-Band Dielectric Spectroscopy on the Molecular Dynamics of Bulk and Adsorbed Poly(Dimethylsiloxane). *Macromolecules* **1993**, *26* (5), 975−980.
(51) Böhmer, R.; Ngai, K. L.; Angell, C. A.; Plazek, D. J. Nonexponential Relaxations in Strong and Fragile Glass Formers. *J. Chem. Phys.* **1993**, *99* (5), 4201−4209.
(52) Alcoutlabi, M.; McKenna, G. B. Effects of Confinement on Material Behaviour at the Nanometre Size Scale. *J. Phys.: Condens. Matter* **2005**, *17* (15), R461−R524.
(53) Huwe, A.; Kremer, F.; Behrens, P.; Schwieger, W. Molecular Dynamics in Confining Space: From the Single Molecule to the Liquid State. *Phys. Rev. Lett.* **1999**, *82* (11), 2338−2341.
(54) Arutkin, M.; Raphaël, E.; Forrest, J. A.; Salez, T. Cooperative Strings and Glassy Dynamics in Various Confined Geometries. *Phys. Rev. E: Stat. Phys., Plasmas, Fluids, Relat. Interdiscip. Top.* **2020**, *101* (3), 1−8.
(55) Kritikos, G.; Karatasos, K. Temperature Dependence of Dynamic and Mechanical Properties in Poly(Acrylic Acid)/Graphene Oxide Nanocomposites. *Mater. Today Commun.* **2017**, *13*, 359−366.
(56) Klein, J.; Kumacheva, E. Confinement-Induced Phase Transitions in Simple Liquids. *Science (Washington, DC, U. S.)* **1995**, *269* (5225), 816−819.
(57) Thompson, P. A.; Grest, G. S.; Robbins, M. O. Phase Transitions and Universal Dynamics in Confined Films. *Phys. Rev. Lett.* **1992**, *68* (23), 3448−3451.
(58) Gang, H.; Müser, M. H.; Robbins, M. O. Adsorbed Layers and the Origin of Static Friction. *Science (Washington, DC, U. S.)* **1999**, *284* (5420), 1650−1652.
(59) Mate, C. M.; Marchon, B. Shear Response of Molecularly Thin Liquid Films to an Applied Air Stress. *Phys. Rev. Lett.* **2000**, *85* (18), 3902−3905.
(60) Cheng, S.; Mirigian, S.; Carrillo, J. M. Y.; Bocharova, V.; Sumpter, B. G.; Schweizer, K. S.; Sokolov, A. P. Revealing Spatially

https://dx.doi.org/10.1021/acs.macromol.0c01040
Macromolecules 2020, 53, 6190−6203

Heterogeneous Relaxation in a Model Nanocomposite. *J. Chem. Phys.* **2015**, *143* (19), 194704.
(61) Kritikos, G.; Terzis, A. F. Variable Density Self Consistent Field Study on Bounded Polymer Layer around Spherical Nanoparticles. *Eur. Polym. J.* **2013**, *49* (3), 613−629.
(62) Behbahani, A. F.; Motlagh, G. H.; Vaez Allaei, S. M.; Harmandaris, V. A. Structure and Conformation of Stereoregular Poly(Methyl Methacrylate) Chains Adsorbed on Graphene Oxide and Reduced Graphene Oxide via Atomistic Simulations. *Macromolecules* **2019**, *52* (10), 3825−3838.
(63) Roussou, R. E.; Karatasos, K. Graphene/Poly(Ethylene Glycol) Nanocomposites as Studied by Molecular Dynamics Simulations. *Mater. Des.* **2016**, *97*, 163−174.
(64) Pandey, Y. N.; Brayton, A.; Burkhart, C.; Papakonstantopoulos, G. J.; Doxastakis, M. Multiscale Modeling of Polyisoprene on Graphite. *J. Chem. Phys.* **2014**, *140* (5), 054908.
(65) Sgouros, A. P.; Vogiatzis, G. G.; Kritikos, G.; Boziki, A.; Nikolakopoulou, A.; Liveris, D.; Theodorou, D. N. Molecular Simulations of Free and Graphite Capped Polyethylene Films: Estimation of the Interfacial Free Energies. *Macromolecules* **2017**, *50* (21), 8827−8844.
(66) Yelash, L.; Virnau, P.; Binder, K.; Paul, W. Three-Step Decay of Time Correlations at Polymer-Solid Interfaces. *Epl* **2012**, *98* (2), 28006.
(67) Falkovich, S. G.; Nazarychev, V. M.; Larin, S. V.; Kenny, J. M.; Lyulin, S. V. Mechanical Properties of a Polymer at the Interface Structurally Ordered by Graphene. *J. Phys. Chem. C* **2016**, *120* (12), 6771−6777.
(68) Batistakis, C.; Lyulin, A. V.; Michels, M. A. J. Slowing down versus Acceleration in the Dynamics of Confined Polymer Films. *Macromolecules* **2012**, *45* (17), 7282−7292.
(69) Pandey, Y. N.; Doxastakis, M. Detailed Atomistic Monte Carlo Simulations of a Polymer Melt on a Solid Surface and around a Nanoparticle. *J. Chem. Phys.* **2012**, *136* (9), 094901.
(70) Rahman, R. The Role of Graphene in Enhancing the Stiffness of Polymeric Material: A Molecular Modeling Approach. *J. Appl. Phys.* **2013**, *113* (24), 243503.
(71) Behbahani, A. F.; Vaez Allaei, S. M.; Motlagh, G. H.; Eslami, H.; Harmandaris, V. A. Structure, Dynamics, and Apparent Glass Transition of Stereoregular Poly(Methyl Methacrylate)/Graphene Interfaces through Atomistic Simulations. *Macromolecules* **2018**, *51* (19), 7518−7532.
(72) Carrillo, J.-M. Y.; Cheng, S.; Kumar, R.; Goswami, M.; Sokolov, A. P.; Sumpter, B. G. Untangling the Effects of Chain Rigidity on the Structure and Dynamics of Strongly Adsorbed Polymer Melts. *Macromolecules* **2015**, *48* (12), 4207−4219.
(73) Daoulas, K. C.; Theodorou, D. N.; Harmandaris, V. A.; Karayiannis, N. C.; Mavrantzas, V. G. Self-Consistent-Field Study of Compressible Semiflexible Melts Adsorbed on a Solid Substrate and Comparison with Atomistic Simulations. *Macromolecules* **2005**, *38* (16), 7134−7149.
(74) Scheutjens, J. M. H. M.; Fleer, G. J. Statistical Theory of the Adsorption of Interacting Chain Molecules. 2. Train, Loop, and Tail Size Distribution. *J. Phys. Chem.* **1980**, *84* (2), 178−190.
(75) Nakatani, A. I.; Chen, W.; Schmidt, R. G.; Gordon, G. V.; Han, C. C. Chain Dimensions in Polysilicate-Filled Poly(Dimethyl Siloxane). *Int. J. Thermophys.* **2002**, *23* (1), 199−209.
(76) Rissanou, A. N.; Papananou, H.; Petrakis, V. S.; Doxastakis, M.; Andrikopoulos, K. S.; Voyiatzis, G. A.; Chrissopoulou, K.; Harmandaris, V.; Anastasiadis, S. H. Structural and Conformational Properties of Poly(Ethylene Oxide)/Silica Nanocomposites: Effect of Confinement. *Macromolecules* **2017**, *50* (16), 6273−6284.
(77) Rissanou, A. N.; Harmandaris, V. Structural and Dynamical Properties of Polystyrene Thin Films Supported by Multiple Graphene Layers. *Macromolecules* **2015**, *48* (8), 2761−2772.
(78) Cornell, W. D.; Cieplak, P.; Bayly, C. I.; Gould, I. R.; Merz, K. M.; Ferguson, D. M.; Spellmeyer, D. C.; Fox, T.; Caldwell, J. W.; Kollman, P. A. A Second Generation Force Field for the Simulation of Proteins, Nucleic Acids, and Organic Molecules. *J. Am. Chem. Soc.* **1995**, *117* (19), 5179−5197.
(79) Wang, J. M.; Wolf, R. M.; Caldwell, J. W.; Kollman, P. A.; Case, D. A. Development and Testing of a General Amber Force Field. *J. Comput. Chem.* **2004**, *25* (9), 1157−1174.
(80) Wang, J.; Wang, W.; Kollman, P. A.; Case, D. A. Automatic Atom Type and Bond Type Perception in Molecular Mechanical Calculations. *J. Mol. Graphics Modell.* **2006**, *25* (2), 247−260.
(81) Stauffer, D.; Dragneva, N.; Floriano, W. B.; Mawhinney, R. C.; Fanchini, G.; French, S.; Rubel, O. An Atomic Charge Model for Graphene Oxide for Exploring Its Bioadhesive Properties in Explicit Water. *J. Chem. Phys.* **2014**, *141* (4), 044705.
(82) Martin, M. G.; Siepmann, J. I. Transferable Potentials for Phase Equilibria. 1. United-Atom Description of n -Alkanes. *J. Phys. Chem. B* **1998**, *102* (97), 2569−2577.
(83) Harmandaris, V. A.; Adhikari, N. P.; Van Der Vegt, N. F. A.; Kremer, K.; Mann, B. A.; Voelkel, R.; Weiss, H.; Liew, C. C. Ethylbenzene Diffusion in Polystyrene: United Atom Atomistic/Coarse Grained Simulations and Experiments. *Macromolecules* **2007**, *40* (19), 7026−7035.
(84) Harmandaris, V. A.; Floudas, G.; Kremer, K. Temperature and Pressure Dependence of Polystyrene Dynamics through Molecular Dynamics Simulations and Experiments. *Macromolecules* **2011**, *44* (2), 393−402.
(85) Steele, W. A. The Physical Interaction of Gases with Crystalline Solids. *Surf. Sci.* **1973**, *36* (1), 317−352.
(86) Hess, B.; Kutzner, C.; Van Der Spoel, D.; Lindahl, E. GROMACS 4: Algorithms for Highly Efficient, Load-Balanced, and Scalable Molecular Simulation. *J. Chem. Theory Comput.* **2008**, *4* (3), 435−447.
(87) Bussi, G.; Donadio, D.; Parrinello, M. Canonical Sampling through Velocity Rescaling. *J. Chem. Phys.* **2007**, *126* (1), 014101.
(88) Berendsen, H. J. C.; Postma, J. P. M.; Van Gunsteren, W. F.; Dinola, A.; Haak, J. R. Molecular Dynamics with Coupling to an External Bath. *J. Chem. Phys.* **1984**, *81* (8), 3684−3690.
(89) Azimi, M.; Mirjavadi, S. S.; Hamouda, A. M. S.; Makki, H. Heterogeneities in Polymer Structural and Dynamic Properties in Graphene and Graphene Oxide Nanocomposites: Molecular Dynamics Simulations. *Macromol. Theory Simul.* **2017**, *26* (2), 1600086.
(90) Güryel, S.; Walker, M.; Geerlings, P.; De Proft, F.; Wilson, M. R. Molecular Dynamics Simulations of the Structure and the Morphology of Graphene/Polymer Nanocomposites. *Phys. Chem. Chem. Phys.* **2017**, *19* (20), 12959−12969.
(91) Anagnostopoulos, G.; Androulidakis, C.; Koukaras, E. N.; Tsoukleri, G.; Polyzos, I.; Parthenios, J.; Papagelis, K.; Galiotis, C. Stress Transfer Mechanisms at the Submicron Level for Graphene/Polymer Systems. *ACS Appl. Mater. Interfaces* **2015**, *7* (7), 4216−4223.
(92) Rissanou, A.; Bacova, P.; Harmandaris, V. Properties of Nanographene in Polymer Nanocomposites through Molecular Simulations: Dynamics and Anisotropic Brownian Motion. *Phys. Chem. Chem. Phys.* **2019**, *21* (43), 23843.
(93) Shen, X.; Lin, X.; Yousefi, N.; Jia, J.; Kim, J. K. Wrinkling in Graphene Sheets and Graphene Oxide Papers. *Carbon* **2014**, *66*, 84−92.
(94) Rissanou, A. N.; Bačová, P.; Harmandaris, V. Properties of Nanographene in Polymer Nanocomposites through All-Atom Simulations: Shape Fluctuations and Rippling. *Comput. Mater. Sci.* **2020**, *172*, 109330.
(95) Whitby, R. L. D.; Gun'ko, V. M.; Korobeinyk, A.; Busquets, R.; Cundy, A. B.; László, K.; Skubiszewska-Zięba, J.; Leboda, R.; Tombácz, E.; Toth, I. Y.; et al. Driving Forces of Conformational Changes in Single-Layer Graphene Oxide. *ACS Nano* **2012**, *6* (5), 3967−3973.
(96) Tang, H.; Liu, D.; Zhao, Y.; Yang, X.; Lu, J.; Cui, F. Molecular Dynamics Study of the Aggregation Process of Graphene Oxide in Water. *J. Phys. Chem. C* **2015**, *119* (47), 26712−26718.

https://dx.doi.org/10.1021/acs.macromol.0c01040
Macromolecules 2020, 53, 6190−6203

(97) Arkin, H.; Janke, W. Gyration Tensor Based Analysis of the Shapes of Polymer Chains in an Attractive Spherical Cage. *J. Chem. Phys.* **2013**, *138* (5), 054904.
(98) Harmandaris, V. A.; Daoulas, K. C.; Mavrantzas, V. G. Molecular Dynamics Simulation of a Polymer Melt/Solid Interface: Local Dynamics and Chain Mobility in a Thin Film of Polyethylene Melt Adsorbed on Graphite. *Macromolecules* **2005**, *38* (13), 5796−5809.
(99) Douglas, J. F. How Does Surface Roughness Affect Polymer-Surface Interactions? *Macromolecules* **1989**, *22* (9), 3707−3716.
(100) Kohlrausch, R. Theorie Des Elektrischen Rückstandes in Der Leidener Flasche. *Ann. Phys.* **1854**, *167* (2), 179−214.
(101) Alvarez, F.; Alegra, A.; Colmenero, J. Relationship between the Time-Domain Kohlrausch-Williams-Watts and Frequency-Domain Havriliak-Negami Relaxation Functions. *Phys. Rev. B: Condens. Matter Mater. Phys.* **1991**, *44* (14), 7306−7312.
(102) Williams, G.; Watts, D. C. Non-Symmetrical Dielectric Relaxation Behaviour Arising from a Simple Empirical Decay Function. *Trans. Faraday Soc.* **1970**, *66* (0), 80.
(103) Ngai, K. L. *Relaxation and Diffusion in Complex Systems; Partially Ordered Systems*; Springer: New York, 2011.
(104) Yelash, L.; Virnau, P.; Binder, K.; Paul, W. Slow Process in Confined Polymer Melts: Layer Exchange Dynamics at a Polymer Solid Interface. *Phys. Rev. E - Stat. Nonlinear, Soft Matter Phys.* **2010**, *82* (5), 050801.
(105) Holt, A. P.; Bocharova, V.; Cheng, S.; Kisliuk, A. M.; Ehlers, G.; Mamontov, E.; Novikov, V. N.; Sokolov, A. P. Interplay between Local Dynamics and Mechanical Reinforcement in Glassy Polymer Nanocomposites. *Phys. Rev. Mater.* **2017**, *1* (6), 062601.
(106) Li, J.; Ding, M.; Zhang, R.; Shi, T. Effects of Surface Roughness on the Self-Diffusion Dynamics of a Single Polymer. *Soft Matter* **2018**, *14* (18), 3550−3556.
(107) Franco, L. F. M.; Castier, M.; Economou, I. G. Anisotropic Parallel Self-Diffusion Coefficients near the Calcite Surface: A Molecular Dynamics Study. *J. Chem. Phys.* **2016**, *145* (8), 084702.
(108) Glor, E. C.; Angrand, G. V.; Fakhraai, Z. Exploring the Broadening and the Existence of Two Glass Transitions Due to Competing Interfacial Effects in Thin, Supported Polymer Films. *J. Chem. Phys.* **2017**, *146* (20), 203330.

https://dx.doi.org/10.1021/acs.macromol.0c01040
Macromolecules 2020, 53, 6190−6203